Analytica Chimica Acta 1403 (2026) 345407

Contents lists available at ScienceDirect

Analytica Chimica Acta

journal homepage: www.elsevier.com/locate/aca

A novel pretreatment strategy for non-aggressive chromium speciation based on a sole bifunctional magnetic ion-imprinted nanocomposite with mild freezing grinding

Yi-Fan Pan [a], Sen Zhang [a], Jing Yang [a], Xiao-Bing Cui [b], Hong-Zhen Lian [a,*]

[a] State Key Laboratory of Analytical Chemistry for Life Science, Jiangsu Key Laboratory of Clean Energy Catalysis and Intelligent Green Chemical Engineering, School of Chemistry & Chemical Engineering and Center of Materials Analysis, Nanjing University, Nanjing, 210023, China
[b] College of Pharmacy, Nanjing University of Chinese Medicine, Nanjing, 210023, China

HIGHLIGHTS

- A magnetic dual-ion imprinted polymer (MDIIP) was developed for Cr species analysis.
- MDIIP adsorbed original Cr(VI)/Cr(III) at different pH without oxidation/reduction.
- Freezing grinding was introduced in pretreatment to preserve Cr species stability.
- Excellent reusability of MDIIP was ascribed to stability of hybrid monolithic layer.
- MDIIP was applied for Cr(VI)/Cr(III) speciation in real-world environmental samples.

GRAPHICAL ABSTRACT

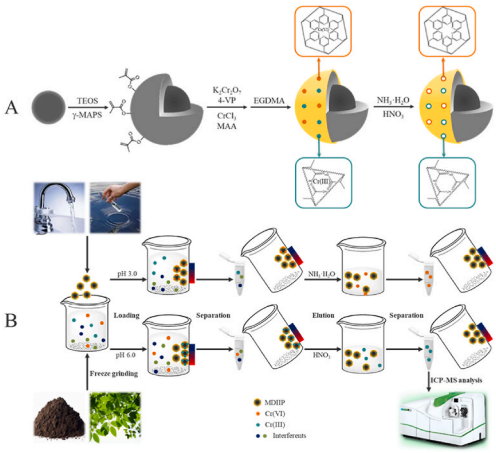

ARTICLE INFO

Handling Editor: Xiu-Ping Yan

Keywords:
Chromium species
Ion-imprinted polymer
Pyridyl- and carboxyl-bifunctionalization
Magnetic solid phase extraction (MSPE)
Freezing grinding

ABSTRACT

Background: The ecological and health effects of chromium depend strongly on its chemical forms. Cr(VI) is hazardous and carcinogenic while Cr(III) sometimes can harm plants and human. Accurate speciation analysis of chromium is therefore essential for environmental monitoring and human health risk assessment. Current analytical methods face issues such as insufficient selectivity of adsorbents, the need for destructive oxidation/reduction steps to change forms, and error propagation caused by indirect calculations through interpolation. Moreover, sample pretreatment methods for solid matrices often neglect the preservation of labile species during processing. These problems seriously hinder the non-destructive speciation analysis of chromium in real samples. *Results:* This work synthesized a novel magnetic pyridyl- and carboxyl-bifunctionalized ion-imprinted nanocomposite by simultaneously grafting 4-vinyl pyridine-$Cr_2O_7^{2-}$ and methylacrylic acid-Cr^{3+} imprinted polymers on the surface of hybrid monolith-decorated Fe_3O_4 cores. Cr(VI) and Cr(III) were specifically adsorbed on the

* Corresponding author.
E-mail address: hzlian@nju.edu.cn (H.-Z. Lian).

https://doi.org/10.1016/j.aca.2026.345407
Received 27 January 2026; Received in revised form 7 March 2026; Accepted 14 March 2026
Available online 17 March 2026

well-characterized bifunctional ion-imprinted polymer (MDIIP) at pH 3.0 and 6.0 as their original status respectively and then eluted by dilute alkaline and acidic solutions followed by ICP-MS detection at enrichment factor of 10 fold. MDIIP showed excellent recognition ability to the target species relative to the competitive anions with similar structures to Cr(VI) and cations with similar ionic radii to Cr(III). The adsorption rate of the magnetic solid phase extraction (MSPE) matrix is still higher than 85% after 5-time use, demonstrating its good reusability attributed to the intermediary hybrid monolith. This DIIP-MSPE-ICP-MS protocol with freezing grinding of samples proved applicable for the speciation analysis of Cr(VI) and Cr(III) in drinking and environmental waters, soil and leaf samples.

Significance: This study reported a magnetic pyridyl- and carboxyl-bifunctionalized ion-imprinted polymer firstly for the simultaneous and non-invasive speciation analysis of Cr(VI) and Cr(III). Notably, a mild freezing grinding operation was utilized for dissolving and extracting Cr(VI) and Cr(III) from complex samples to keep them intact before MSPE separation and enrichment. Consequently, the bifunctionalized ion-imprinted nanocomposite promises a desirable prospect in the separation and enrichment of inorganic chromium species.

1. Introduction

Chromium is widely used in light and heavy industrial fields such as dyes, leather tanning, and electroplating, etc. Chromium-containing wastes are inevitably generated during the industrial process, and they will contaminate the natural water and soil through wastewater, exhaust gas and other channels. Long-term uptake of drinking water with excessive chromium than the maximum contamination limit (MCL) will cause cancer, liver and kidney damage, etc., and even low-level exposure may lead to chronic poisoning and health hazards [1,2]. The chromium in the soil is absorbed by plants and crops, and eventually enters the human body, causing harm to humans. Besides, high levels of chromium in the soil results in the decomposition of chlorophyll in plants, affecting the normal life activities of plants [3]. Therefore, chromium pollution in the environment has been a major concern [4,5].

Chromium lies in the natural environment in the valent states of −2∼+6, mainly in hexavalent Cr(VI) and trivalent Cr(III) forms [6]. Cr (VI) exists mainly in the species of neutral molecule H_2CrO_4 and oxygen anions ($HCrO_4^-$, CrO_4^{2-} and $Cr_2O_7^{2-}$). Cr(VI), as a Class I carcinogen, is the assignable cause of DNA damage, genome instability, genetic disorders and cell malignant transformation in animals and humans [7–10]. Besides, Ali et al. found that the Cr(VI) in soil significantly increased the content of malondialdehyde (MDA) in wheat, reducing the photosynthesis rate and inhibiting its growth and development [11]. WHO [12] and China [13] have set MCL of hexavalent chromium in drinking water at 0.05 mg L^{-1}, although EPA [14] proposed a MCL of 0.1 mg L^{-1} earlier. In addition, China [15] has set a MCL of hexavalent chromium in residential land, park green land and other urban construction lands with dense human activities at 30 mg kg^{-1}. In contrast, Cr(III) exists mainly in the species of Cr^{3+}, $Cr(OH)^{2+}$, $Cr(OH)_2^+$, $Cr(OH)_3$ and $Cr(OH)_4^-$. Cr (III) is considered an essential trace element that plays a crucial role for glucose metabolism in vertebrates and for proper human physiological [16,17]. However, some studies have shown that higher concentrations of Cr(III) in soil can inhibit plant growth by inhibiting plant photosynthesis [18,19], and several toxicological studies have confirmed that Cr (III) can cause chromium allergies and exert a damaging effect on DNA [20,21]. For the foregoing reasons, therefore, detecting the species and their level of chromium present in the environment is very important to provide a more scientific and comprehensive evaluation of quality safety of the ecosystem and health risks to the population.

Since atomic spectroscopy including graphite furnace atomic absorption spectrometry and atomic fluorescence spectrometry, and elemental mass spectrometry including inductively coupled plasma-mass spectrometry (ICP-MS) can only determine the total content of elements but not distinguish their forms at the current stage, elemental speciation analysis usually requires a combination of separation and detection. Commonly used separation techniques are divided into chromatographic and non-chromatographic protocols [22–33]. As a special solid phase extraction (SPE) technology, magnetic solid phase extraction (MSPE) based on magnetic nanocomposites possesses a lot of merits such as easy operation, fast separation, good reusability and environment friendship, which has been widely employed for separation and enrichment of metals/metalloids and their species in recent years [25,27,33].

Given the distinct physical, chemical, and toxicological properties of Cr(VI) and Cr(III), their speciation and removal require adsorbents tailored for high performance in selectivity, enrichment factor, adsorption capacity, and recovery. This necessity has driven the investigation of diverse materials for inorganic chromium separation. In general, mono-functional SPE materials can adsorb Cr(VI) or Cr(III) species of chromium at different pH. For example, Yan's group performed the magnetic immobilization of amino-functionalized magnetic nanoparticles (MNPs) onto the inner walls of a knotted reactor for on-line SPE for speciation analysis of Cr(VI) and Cr(III) under pH 2.7 and 10.5, respectively [24]. Shirkhanloo et al. reported an ultrasound-assisted heterogeneous suspension ionic-liquid micro-solid-phase extraction method based on N-benzyl-N-methyl thiourea immobilized on multi-walled carbon nanotubes (MWCNTs) for the speciation and determination of Cr(III) and Cr(VI) in water and food samples under pH 5.5 and 2.5, respectively [26]. Some mono-functional materials can only act on one specie, and the other is determined by redox conversion. Ahmed et al. synthesized MWCNTs based MWCNTs@$CuAl_2O_4$@SiO_2 nanocomposite and utilized it to extract Cr(VI) as ammonium pyrrolidinedithiocarbamate (APDC) chelate. Potassium permanganate ($KMnO_4$) was used to oxidize Cr(III) to Cr(VI), and the protocol was applied to determine the total chromium. The concentration of Cr(III) was obtained by finding differences between total chromium and Cr(VI) [34]. Erbas et al. reported an MSPE method for the separation-preconcentration and speciation of chromium. The scheme is based on the adsorption of Cr(VI)-APDC complex on the activated charcoal@$MoSe_2$@Fe_3O_4 composite. Total chromium also was determined after the conversion of Cr(III) to Cr(VI) by $KMnO_4$ oxidation, and Cr(III) was calculated as the difference [35]. However, there are three main problems in the above methods. (1) Relying solely on the differential attraction forces of a single functional group at varying pH levels typically yields insufficient separation selectivity for effectively distinguishing between different species of the same element. (2) Severe $KMnO_4$ oxidation may cause the destruction of other chromium forms (e.g., organic chromium species) in the original samples, and the use of high valent metal-containing oxidizing agents introduce other metal ions that probably interfere with the reliability of speciation analysis. (3) The content of the alternative species is determined indirectly by subtraction. This approach entails an additional pretreatment step and can propagate unavoidable analytical errors into the final result. Researchers have a taste for the combined use of two monofunctional materials. Silva et al. synthesized two kinds of MWCNTs modified with methacrylic acid (MAA) (MWCNT-PMAA) and 4-vinylpyridine (4-VP) (MWCNT-P4VP), respectively, packed in two mini-columns made of polyethylene. When Cr(III) was retained onto MWCNT-PMAA, Cr(VI) is eluted from MWCNT-P4VP using HNO_3. By switching the central part of injector, the elution of Cr(III) is carried out and Cr(VI) is again preconcentrated into MWCNT-P4VP [36]. In this work, a couple of

adsorbents need to be prepared and then packed into different columns assembled together by a switchable device to adsorb two chromium species respectively, which is somewhat cost-increasing and laborious.

Throughout the last over a decade, the limitations of mono-functionalized materials have prompted the development of multi-functionalized materials for chromium speciation. Even so, there have been a few doubly functionalized materials being reported. Zhao et al. developed an amine- and carboxyl-bifunctionalized hybrid monolithic column (HMC), with good performance to ensure the efficiency of separation for Cr(VI) and Cr(III), and utilized it as a needle-SPME matrix for direct enrichment of the individual target species, with no oxidation/reduction treatment [37]. This organic-inorganic hybrid monolith in-situ prepared within HMC by sol-gel method integrates the merits of traditional inorganic silica and organic polymer monoliths, especially with high mechanical and chemical stability. Faisal et al. proposed an amine- and carboxyl-bifunctionalized magnetic nanocomposite and used it as magnetic MSPE adsorbent to separate and enrich Cr(VI) and Cr (III) with strong anti-interference ability from the two labile species each other [33]. However, all of the functionalized materials mentioned above adsorbed the inorganic chromium species only by electrostatic or coordination interaction, which will inevitably attract other interfering substances with the same interaction in the analyzed samples.

Ion imprinting technology (IIT) is an offshoot of molecular imprinting technology (MIT). IIT uses target ions as templates, and combines them with functional monomers through coordination or electrostatic attraction, etc. The functional monomers surround and fix the template, and then polymerize with a cross-linker to prepare ion-imprinted polymers (IIPs). Finally, the templates are removed by solvent elution, leaving imprinted holes with specific recognition sites in the polymers. There are two significant advantages in IIPs. The imprinted cavities with specific structures have super high selectivity for target ions. Under many circumstances, the target ions interact with the functional monomers first and then polymerize, which is beneficial to maintaining the stability of the target ions especially for labile elemental species ions during the reaction [38–42].

In recent years, surface imprinting technology has become a frequently employed strategy for preparing IIPs. It is a technology that performs polymerization reaction on the surface of solid matrices so that the recognition sites of target ions are evenly dispersed on the surface of the supporters. IIPs prepared by this method has a fast binding rate between target ions and specific recognition cavities and sites, high separation efficiency, and less embedding phenomenon. Due to the specific recognition and enrichment of ions, surface IIPs have been applied to the separation and analysis of elements and their species [43–45]. Liu et al. used 3-aminopropyltriethoxysilane (APTES) and Cr^{3+} to form a composite template, and introduced tetraethyl orthosilicate (TEOS) as silane coupling agent to prepare a Cr(III)-imprinted polymer on the surface of silica mesoporous material. Cr(III) and the total chromium concentrations after reducing Cr(VI) to Cr(III) by hydroxylamine hydrochloride were determined by ICP-AES, the Cr(VI) concentration was then calculated by subtracting the Cr(III) from the total chromium, and at the same time the remainder of Cr(VI) in the solution was validated by UV-vis spectroscopy [46]. Ma's group prepared a Cr(VI) ion-imprinted polymer (Cr(VI)-IIP) on the surface of graphene oxide-mesoporous silica (GO-MS) nanosheets with 3-(2-aminoethylamino) propyl trimethoxysilane (AAPTS) as the functional monomer. The prepared Cr(VI)-IIP was applied to remove Cr(VI) ions from aqueous solution, and the concentration of Cr(VI) was detected by FAAS [47]. Kong et al. proposed a “pre-grafting and post-imprinting” method for synthesis of polypropylene (PP) fiber-based Cr(VI)-IIPs through specific steps including grafting of 2-(dimethylamino)ethyl methacrylate (DMAEMA) onto the inexpensive PP fibers by high electron beam irradiation graft polymerization, and functionalization of quaternary ammonium with epichlorohydrin (ECH), and Cr(VI) imprinting. The initial and final concentrations of Cr(VI) in solution were determined by UV-vis spectrophotometry as 1,5-diphenylcarbohydrazide complex of Cr (VI) [48]. In addition, Magnetic Cr(VI)-imprinted nanoparticles (Fe_3O_4@Cr(VI)-IIPs) were prepared by hyphenating surface ion-imprinted with sol–gel techniques. During the preparation process, vinylimidazole (1-VIA) and APTES were used as organic functional monomer and comonomer respectively, while methacryloxypropyltrimethoxysilane (γ-MAPS) selected as the coupling agent. A dispersive SPE, i.e., MSPE method was proposed for the extraction and enrichment of Cr(VI) prior to FAAS [49]. So far, however, there have been not any reports about the multi-functionalized ion-imprinted polymers for simultaneous separation of different species of same an element, especially for inorganic chromium species.

Sample preparation is an important part not only in trace heavy metal analysis but also in their elemental speciation. However, most pretreatment methods in existing reports do not pay enough attention to the originality, stability and transformation of labile element species. Shan's group studied water soluble, exchangeable and carbonate bound (B1), Fe–Mn oxide bound (B2), organic matter and sulfide bound (B3) of heavy metals (Cu, Pb, Cr, Cd, Zn and Ni) in reservoir surface sediments [50]. Although chromium was involved, Cr(VI) and Cr(III) were not specifically discussed but treated as a whole. In this work, the effect of different drying methods (oven-drying at 85 °C, air-drying at 20 °C, and freeze-drying) on metal fractionation distribution was investigated, and they observed that whatever the drying methods would influence the fractionation distribution of trace metals and the changes brought by air-drying and freeze-drying methods were minimal. In our present work, since soil and leaf samples are large in size and need to be crushed before extraction, freezing grinding should be a good choice.

Current speciation analysis methods face issues such as non-specificity of adsorbents, the need for destructive oxidation/reduction steps to change forms, and error propagation caused by indirect calculations through interpolation. Moreover, sample pretreatment methods for solid matrices often neglect the preservation of labile species during processing.

Therefore, we designed and prepared a magnetic nanoparticles containing both Cr(VI) and Cr(III) ion-imprinted polymers, MDIIP for short. The synthesis of MDIIP involved the solvothermal generation of Fe_3O_4 nanoparticles, followed by the sol-gel synthesis of an organic-inorganic hybrid material to produce vinyl-functionalized Fe_3O_4 (Fe_3O_4@HM), and free radical polymerization reaction for preparing 4-vinyl pyridine-$Cr_2O_7^{2-}$ (4-VP-$Cr_2O_7^{2-}$) and methylacrylic acid-Cr^{3+} (MAA-Cr^{3+}) bifunctionalized IIPs on the surface of Fe_3O_4@HM. The as-prepared polymer offered specific imprinting cavities and sites of both Cr(VI) and Cr(III), relatively fast adsorption-desorption rate, as well as magnetic responsiveness. In addition, the resultant hybrid monolithic (HM) interlayer endowed the MDIIP with stable chemical property and firmly rigid configuration. On the other hand, liquid nitrogen freezing grinding was carried out at 15 cycles for pretreating soil and leaf in order to maintain the originality of native species of chromium. The obtained soil and leaf powder samples were accurately weighed and extracted for inorganic chromium species using ultrapure water under shaking. The MDIIP served as a selective MSPE sorbent for inorganic chromium speciation. This method enabled direct, non-destructive analysis of complex samples (waters, soil, and leaves) with subsequent quantification by ICP-MS.

2. Materials and methods

The reagents, materials, samples and apparatus used in this work were described in detail in Supplementary Material Text S1.1 and S1.2.

2.1. Synthesis of MDIIP

The synthesis route from Fe_3O_4 to Fe_3O_4@HM and then to Fe_3O_4@HM@N–Cr(VI)–COOH–Cr(III), i.e. MDIIP, is presented schematically in Fig. 1A. Fe_3O_4 nanoparticles were prepared via solvothermal method, and hybrid silane coated Fe_3O_4 nanoparticles

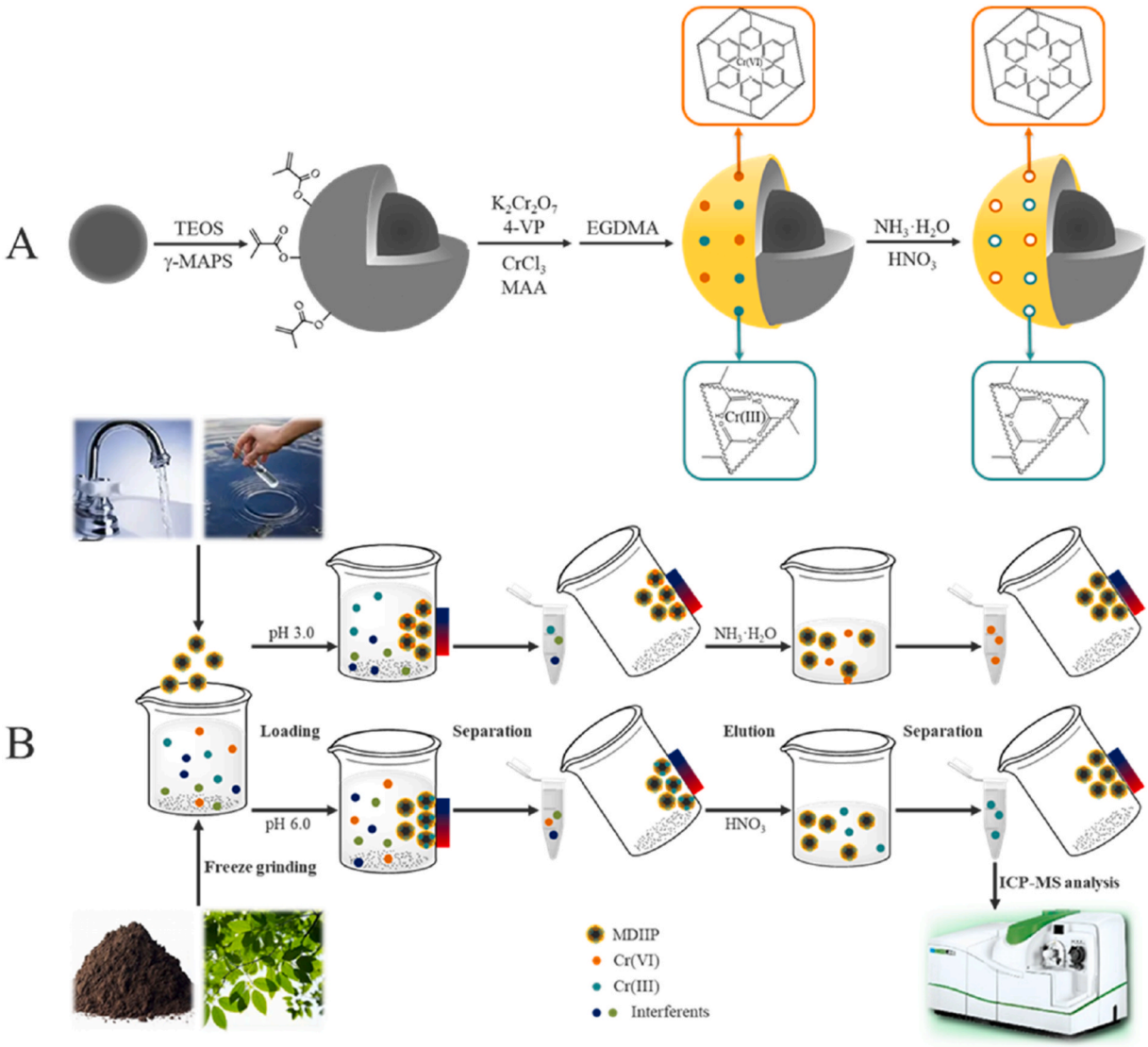

Fig. 1. Schematic diagrams of synthesis process of MDIIP (A). Speciation analysis procedure of Cr(VI) and Cr(III) by DIIP-MSPE-ICP-MS (B).

(Fe_3O_4@HM) were obtained by sol-gel method as stated in Text S1.3 and S1.4.

Cr(III) and Cr(VI) ion imprinted polymers were grafted onto Fe_3O_4@HM surface via free radical polymerization reaction as described below. Firstly, 5 mg mL^{-1} Cr(VI) and Cr(III) aqueous solutions were prepared with $K_2Cr_2O_7$ and $CrCl_3·6H_2O$, respectively. Then, Cr(VI) solution (2 mL), 4-VP (2 mL) and absolute ethanol (2 mL) were mixed and shook for 1 day for pre-polymerization, and Cr(III) solution (2 mL), MAA (2 mL) and absolute ethanol (2 mL) were mixed and shook for 1 day for pre-polymerization. Subsequently, the above two stabilized templet species ions by electrostatic and complexing interactions respectively with 4-VP and MAA, as well as EGDMA (1.4 mL) and AIBN (100 mg) were dispersed in 150 mL ethanol, and 0.4 g Fe_3O_4@HM were added into the mixture with sonication for 10 min. After the mixture was transferred to a flask, the reaction was performed with stirring in nitrogen atmosphere at 60 °C for 24 h. The obtained MDIIP nanocomposites were separated from the resulting solution by a magnet, washed with 1.0 mol L^{-1} $NH_3·H_2O$ and 10% HNO_3 (v/v) several times for removing Cr(VI) and Cr(III) respectively, until no chromium ion was detected in the supernatant by ICP-MS, and finally dried under vacuum at 60 °C overnight. In the meantime, non-imprinted polymer grafted Fe_3O_4@HM (Fe_3O_4@HM@N–COOH, i.e. MDNIP, was prepared with the same procedures as above described without adding two kinds of chromium ions. A single imprinted polymer containing only Cr(VI) (Fe_3O_4@HM@N–Cr(VI), MSIIP-Cr(VI) for short) was prepared by adding Cr(VI) and 4-VP, and another single imprinted polymer containing only Cr(III) (Fe_3O_4@HM@COOH–Cr(III), MSIIP-Cr(III) for short) was also prepared only adding Cr(III) and MAA. To our best knowledge, this is the first attempt to prepare bifunctionalized ion-imprinted nanocomposites for elemental speciation.

2.2. Speciation analysis process

The DIIP-MSPE-ICP-MS protocol for the enrichment of Cr(VI) and Cr(III) is shown in Fig. 1B. The separation of two kinds of chromium species was performed by a “step by step” loading and elution strategy, and the detailed operation processes are as follows. In adsorption step, 5 mL aqueous solution containing Cr(VI) was adjusted to pH 3.0 by adding HNO_3 or $NH_3·H_2O$ solutions, and 5 mg of MDIIP nanoparticles were added to the sample solution as MSPE adsorbents. After this solution was shook for 40 min to reach adsorption equilibrium, MDIIP loaded with Cr(VI) (MDIIP + Cr(VI)) was isolated by a magnet. In desorption step, after rinsing with loading solvent at pH 3.0, Cr(VI) adsorbed on MDIIP was eluted by 0.5 mL 1.0 mol L^{-1} $NH_3·H_2O$ under continuous shaking for 10 min, and the supernatant was determined by ICP-MS. The adsorption-elution process of Cr(III) was modified in only two places, the pH of

Cr(III) aqueous solution before adsorption was adjusted to pH 6.0, and Cr(III) adsorbed on MDIIP was eluted by 0.5 mL 10% HNO_3 (v/v) after rinsing with loading solvent at pH 6.0.

2.3. Pretreatment of actual samples

All water samples were stored at 4 °C refrigerator and filtered through a 0.45 μm cellulose acetate membrane prior to use. Soil and leaf samples were ground directly into powders by a liquid nitrogen freezing grinder for 15 cycles. When using, 1.000 g soil or leaf powder sample was weight accurately and added to 50 mL ultra-pure water. The mixture was shook at a speed of 100 rpm for 12 h to extract chromium species without destroying the original forms as far as possible.

3. Results and discussion

3.1. Characterizations of magnetic nanocomposites

3.1.1. Morphology and structure

The morphology including shape and size of the prepared magnetic nanocomposites were characterized by using transmission electron microscopy (TEM). As shown in Fig. 2, MDIIP and MDNIP were of quasi-spherical shape, with average diameters of 200 and 160 nm, respectively. The dimensional homogeneity was attributed to the Fe_3O_4 nanoparticles generated through solvothermal reaction as the cores. In Fig. 2, the dark spheres in the middle were Fe_3O_4 nanoparticles Moreover, the core-shell structural Fe_3O_4@HM nanoparticles were embedded with translucent polymer layers in a uniform thickness of about 5 nm in MDIIP (Fig. 2A and C) and MDNIP (Fig. 2B and D). The visibly rough interfaces between Fe_3O_4 cores and polymer layers were due to the presence of organic-inorganic hybrid monolith. It can also be observed that the introduction of the template ions made the surface of MDIIP looser than MDNIP. Furthermore, the existence of C, N, O, Si, Cr and Fe in MDIIP without eluting Cr(VI) and Cr(III) templates and MDNIP was analyzed by elemental mapping (Fig. S1), which suggested sol-gel and free radical polymerization reactions occurred on the surface of Fe_3O_4, with the implantation of chromium species templates.

3.1.2. Surface functional groups

The infrared spectra of Fe_3O_4@HM, MDIIP and MDNIP are represented in Fig. 3A. The absorption peaks at about 580, 1095 and 1390 cm^{-1} in all three spectra were assigned to the stretching vibrations of Fe–O, Si–O and C–C bonds, respectively. The peaks at 1140 and 1720 cm^{-1} of MDIIP and MDNIP come respectively from the stretching vibrations of C–O and C═O bonds in MAA carboxyl group and EGDMA ester group. The peak around 1418 cm^{-1} is ascribed to C–N stretching vibration of 4-VP, while those at 1600 and 3065 cm^{-1} are the characteristic absorption of pyridine ring, which together indicate that the functional monomer 4-VP was polymerized in the formed polymer. The great increase in intensity of C–C absorption at 1390 cm^{-1} in the two spectra compared to Fe_3O_4@HM further supported the involvement of MAA and EGDMA into the consequential formation of polymer layer. Therefore, all the FT-IR results confirmed the successful preparation of DMIIP and DMNIP.

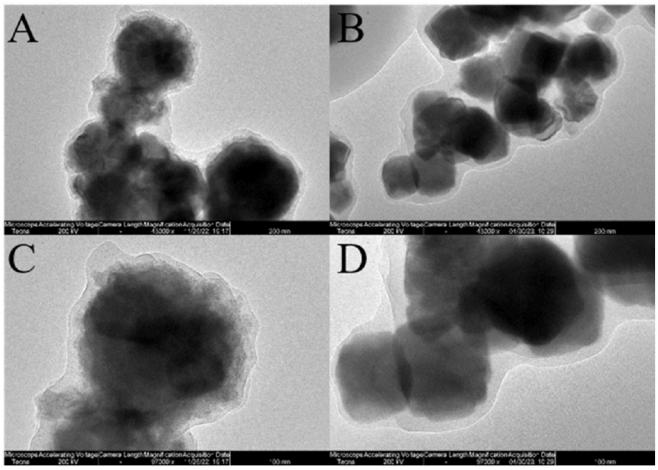

Fig. 2. TEM images of MDIIP (A,C) and MDNIP (B,D).

3.1.3. Crystal form

The X-ray diffraction (XRD) patterns of Fe_3O_4, Fe_3O_4@HM and MDIIP are illustrated in Fig. 3B. Six main diffraction peaks were observed in the three materials at the indices (220), (311), (400), (422), (511) and (440), which corresponded to the standard XRD data card of Fe_3O_4 crystal (JCPDS No. 19-0629) as we reported earlier [33]. The results reminded that the high crystalline state of Fe_3O_4 remained unchanged during the stepwise synthesis.

3.1.4. Thermal stability

The thermogravimetric analysis (TGA) curves of Fe_3O_4, Fe_3O_4@HM and MDIIP are shown in Fig. 3C. Fe_3O_4 nanoparticles had good thermal stability throughout the test temperature range without obvious weight loss. The TGA curve of Fe_3O_4@HM was similar to that of Fe_3O_4 before 310 °C. Thereafter, it displayed a slight weight loss up to 800 °C, which might result from the escape or degradation of unreacted reagents like TEOS and γ-MAPS. This excellent thermal stability was originated from the firmly rigid configuration of organic-inorganic hybrid monolith wrapping Fe_3O_4 cores. As for MDIIP, the weight loss before 120 °C was attributed to the vaporization of micro amount water and organic solvents such as ethanol remained on the surface, and then a much sharper weight-loss occurred from 250 to 420 °C due to the degradation of the polymer layer.

3.1.5. Magnetism

Strong magnetism is important for MSPE separation of target analytes in solution. The magnetisms of Fe_3O_4, Fe_3O_4@HM, MDIIP and MDNIP were measured and their hysteresis loops are shown in Fig. 3D, with the saturation magnetization values of 72.4, 64.93, 37.10 and 31.05 $emu \cdot g^{-1}$, respectively. The gradual decrease in magnetic intensity was ascribed to the stepwise coating of hybrid silane and ion-imprinted polymers. Despite this, it was still easily attracted by a magnet in a few seconds.

3.1.6. Surface electrical property

The zeta potentials were determined to inspect the net surface charges of Fe_3O_4, Fe_3O_4@HM and MDIIP from pH 1.0 to 10.0 as shown in Fig. S2. The dependence of zeta potential of Fe_3O_4 upon pH was similar to our previous report with the isoelectric point (IEP) of pH 5.7 [51]. The IEPs of Fe_3O_4@HM and MDIIP were 5.1 and 4.7, respectively, which reflected the surface modification on the magnetic nanoparticles with TEOS and γ-MAPS, and then 4-VP, MAA and EGDMA. In addition, pyridyl-functionalized (MSIIP-Cr(VI)) and carboxyl-functionalized ion-imprinted magnetic nanocomposites (MSIIP-Cr(III)) were prepared individually. The IEPs of these two single-functionalized MSIIP-Cr(VI) and MSIIP-Cr(III) after eluting the template species were 5.0 and 4.4 respectively, and the IEP of MDIIP was right in between. This result is due to the concurrent decoration of tertiary amino and carboxyl groups.

3.1.7. Surface chemical property

X-ray photoelectron spectroscopy (XPS) was utilized for the characterization of MDIIP before and after removing Cr(VI) and Cr(III) templates by sequentially elution with dilute $NH_3 \cdot H_2O$ and HNO_3 solutions. Fig. S3A shows that there was Cr 2p peak in the spectra of MDIIP before elution. The detail Cr 2p spectrum can be deconvoluted into seven peaks in the upper-left inset, in which, 576.0, 580.0 and 586.3 eV were assigned to the binding energies of CrO_4^{2-}, and 576.1, 578.5, 582.5

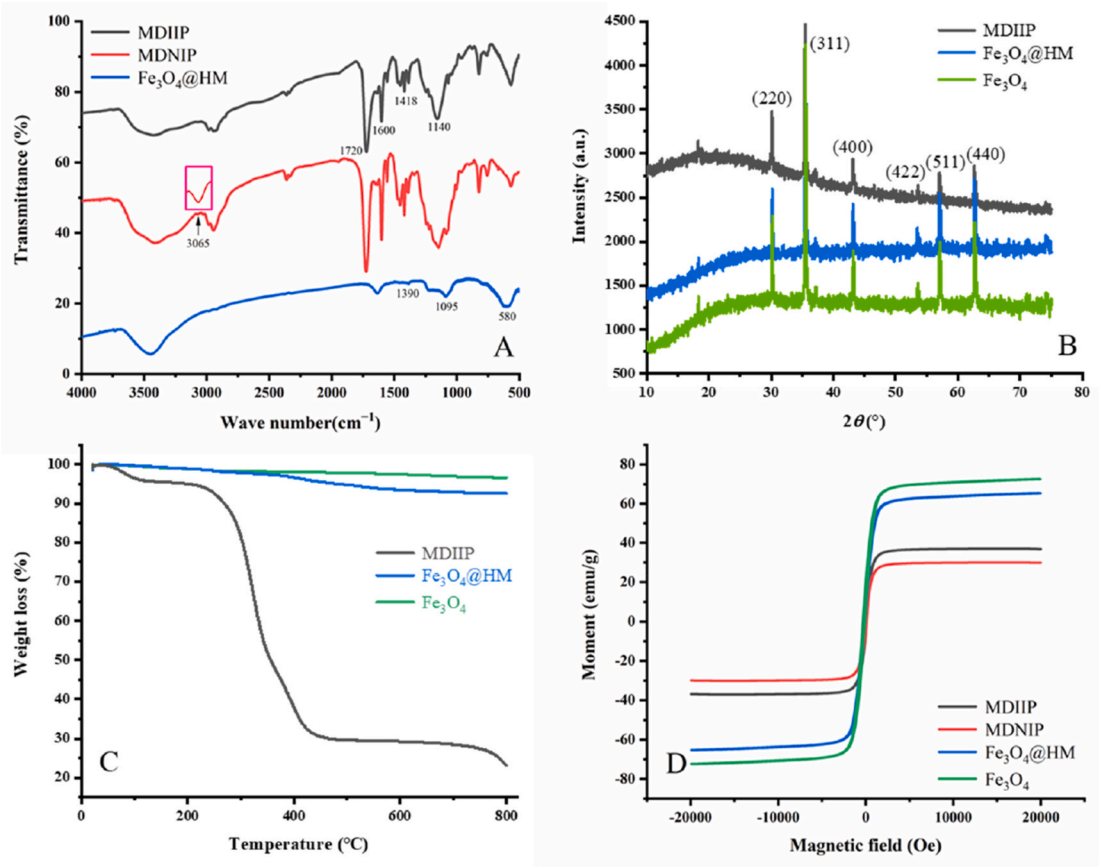

Fig. 3. FT-IR spectra of Fe_3O_4@HM, MDIIP and MDNIP (A). XRD patterns of Fe_3O_4, Fe_3O_4@HM and MDIIP (B). TGA curves of Fe_3O_4, Fe_3O_4@HM and MDIIP (C). Magnetization curves of Fe_3O_4, Fe_3O_4@HM, MDIIP and MDNIP (D).

and 588.5 eV to $Cr(CO)^{3+}$, $Cr(H_2O)^{3+}$, Cr^{3+}–N and Cr^{3+} respectively. After elution, the Cr 2p spectrum disappeared as shown in Fig. S3B. It was proved that two chromium species were introduced and removed, respectively, before and after the elution.

3.2. Effect of loading conditions on adsorption performance

3.2.1. Solution pH

The pH of the solution has a significant effect on the adsorption performance of MDIIP and MDNIP towards inorganic chromium species. The details of the batch experiments were described in Supplementary Material Text S1.5. As shown in Fig. 4A, as the pH of Cr(VI) solution increased from 1.0 to 3.0, the adsorption rates of MDIIP and MDNIP towards Cr(VI) increased rapidly. However, when the pH was raised further from 3.0 to 6.0, the adsorption rates decreased sharply. This phenomenon can be explained as follows. The tertiary amino groups in the pyridine ring of 4-VP are protonated under strong acidic medium because the dissociation constant (pK_a) of 4-VP is 5.4, while Cr(VI) is

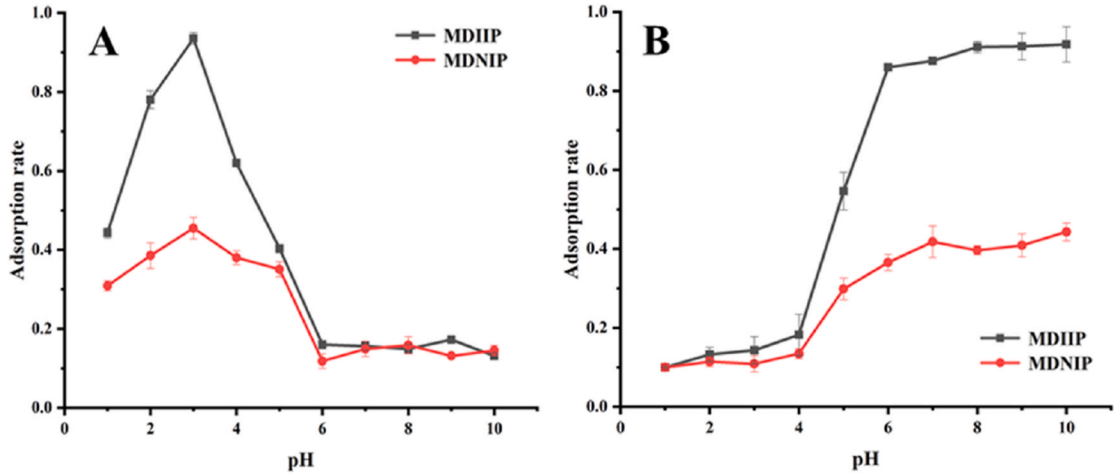

Fig. 4. Influence of solution pH on adsorption rates of Cr(VI) (A) and Cr(III) (B) onto MDIIP (black line) and MDNIP (red line). Dose of adsorbent: 5.0 mg; concentration of Cr(VI) or Cr(III): 50 μg L^{-1}; sample volume: 5 mL; extraction time: 40 min. (For interpretation of the references to colour in this figure legend, the reader is referred to the Web version of this article.)

present in a neutral molecule H_2CrO_4 in aqueous solutions at pH < 1 [52]. Therefore, the electrostatic attraction between neutral Cr(VI) molecule and protonated tertiary amino groups in 4-VP is very weak on this occasion [53]. When the pH is greater than 1.0, Cr(VI) exists as anions, $HCrO_4^-$, CrO_4^{2-} and/or $Cr_2O_7^{2-}$ [52], and strongly binds protonated tertiary amino groups. Once the pH was greater than 6.0, the adsorption amount of Cr(VI) onto MDIIP approached minimized. This is because the tertiary amino groups are electrically neutral, and electrostatic interactions between 4-VP and Cr(VI) almost disappear. As shown in Fig. 4B, when the pH of Cr(III) solution increased from 1.0 to 4.0, the adsorption rates of MDIIP and MDNIP towards Cr(III) increased slowly. The monovalent carboxyl group of MAA with pK_a value of 4.6 is mainly present as neutralized –COOH under strong acidic medium, while Cr(III) mainly exists in the forms of Cr^{3+}, $Cr(OH)^{2+}$ and $Cr(OH)_2^+$ at pH < 6 [54]. Therefore, the electrostatic attraction of neutral MAA towards cationic Cr(III) is very weak. The slight increase in adsorption rates of MDIIP and MDNIP towards Cr(III) is attributed to the slow increase of coordination interaction between the oxygen atom of –COOH and Cr(III) cations with the increasing pH. However, when the pH was raised from 4.0 to 6.0, the adsorption rates increased sharply. This is because the increasing electrostatic interaction between the dissociated carboxyl group ($–COO^-$) and cationic Cr(III). Meanwhile, the coordination interaction between the oxygen atom of –COOH and Cr(III) cations contributes to the adsorption. As the pH further raised, the adsorption rates continued to slightly increase, although the Cr(III) is mainly present in $Cr(OH)_3$ and $Cr(OH)_4^-$ at pH > 6 [54]. This is because the coordination interaction between –COOH in MAA and Cr(III) cations predominate the binding forces in weak acidic and alkaline media. In addition, there may also be coordination interaction between neutral tertiary amino groups in pyridine ring of 4-VP and Cr(III) cations as the existence of Cr^{3+}–N in above XPS measurement (Fig. S3A, inset). Under the pH far higher than 6.0, however, Cr(III) is inclined to precipitate and the chromium concentration detected in the supernatant after adsorption probably becomes lower than it is, which may results in false high adsorption rate. Compared with MDNIP, MDIIP has a higher adsorption rate, due to the specific geometric structure towards Cr(VI) and Cr(III). Compromisingly, the solution pH for the adsorption of Cr(VI) and Cr(III) on MDIIP as well as MDNIP were selected as 3.0 and 6.0, respectively, for the subsequent loading experiments.

3.2.2. Adsorbent dosage

In order to obtain the maximum adsorption efficiency at minimal cost, the effect of the quantity of the magnetic bifunctionalized ion-imprinted polymer, MDIIP, on the adsorption performance of inorganic chromium species was optimized through the batch experiments as described in Text S1.6. It can be seen from Fig. S4 that the adsorption rates of Cr(VI) and Cr(III) increased gradually as the quantity of MDIIP was increased from 1.0 to 5.0 mg. With greater mass of the adsorbent, more active groups and imprinted holes are involved in the adsorption process, and a greater number of chromium species can be adsorbed. When 5.0 mg or more adsorbent were used, the adsorption rates did not change much. Thereby, a MDIIP amount of 5.0 mg was adopted in loading operation.

3.2.3. Adsorption selectivity

The selectivity of MDIIP towards Cr(VI) and Cr(III) was investigated and the details were presented in Text S1.7. Table 1 summarizes the distribution ratio (K_d), selectivity coefficient (K) and relative selectivity coefficient (K') calculated via their equations, respectively, summarized in Text S1.7. As can been found from Table 1, the distribution ratios of Cr (VI) and Cr(III) on MDIIP was far greater than that on MDNIP under the respective conditions. In addition, compared to Cr(VI) and Cr(III), MDIIP had a lower adsorption capacity to the six competing metal ions. The selectivity coefficients of MDIIP for Cr(VI)/Mn(VII), Cr(VI)/As(III), Cr(VI)/Au(III), Cr(III)/Mg(II), Cr(III)/Ni(II) and Cr(III)/Zn(II) were higher than those of MDNIP, which means that MDIIP possess much better selectivity for Cr(VI) and Cr(III) respectively compared to the competing metal ions. The specific geometric structure of the imprinted cavities in the MDIIP is responsible for these properties, owing to its high selective binding affinity for Cr(VI) and Cr(III). As a measure of relative adsorption ability towards the imprinted ion, the relative selectivity coefficients of MDIIP for them were calculated to be 4.49, 1.59, 2.02, 2.86, 6.14 and 3.73 times higher than MDNIP, respectively.

Table 1
Adsorption selectivity of MDIIP and MDNIP towards Cr(VI) against Mn(VII), As (III) and Au(III), and that towards Cr(III) against Mg(II), Ni(II) and Zn(II).

Ions	+/−	K_d		K		K'
		MDIIP	MDNIP	MDIIP	MDNIP	
Cr(VI)	-	40.30	15.07			
Mn(VII)		0.25	0.42	161.20	35.88	4.49
As(III)		8.76	5.22	4.60	2.89	1.59
Au(III)		9.66	0.73	4.17	2.06	2.02
Cr(III)	+	34.29	9.77			
Mg(II)		0.28	0.23	122.98	42.94	2.86
Ni(II)		0.19	0.33	181.37	29.55	6.14
Zn(II)		0.32	0.34	107.16	28.73	3.73

3.2.4. Adsorption isotherm

The isotherm model can further reflect the interaction mechanism between MDIIP adsorbent and chromium species ions. Langmuir and Freundlich models were used to fit the measurement data in this work. The details of adsorption experiments are presented in Text S1.8. As shown in Fig. S5, the maximum adsorption capacities of MDIIP for Cr (VI) and Cr(III) were 5.673 and 4.692 mg g^{-1}, respectively, which are higher than those of MSIIP-Cr(VI) for Cr(VI) and MSIIP-Cr(III) for Cr(III). And in Table S2, the coefficient of determination (R^2) of the MDIIP for the Langmuir model (0.957 and 0.990 for Cr(VI) and Cr(III)) are respectively better than those for the Freundlich model (0.813 and 0.965 for Cr(VI) and Cr(III)) in describing the adsorption process. This indicates that the adsorption of these two chromium species was a uniform and single-layer chemical adsorption process.

3.2.5. Adsorption kinetics

The pseudo-first-order and pseudo-second-order adsorption kinetic models were used to fit the measurement data based on the adsorption experiments in Text S1.9. As shown in Fig. S6, the R^2 values for pseudo-second-order model (0.9963 and 0.9888 for Cr(VI) and Cr(III)) are respectively better than those for pseudo-first-order model (0.9656 and 0.9333 for Cr(VI) and Cr(III)), being closer to 1 in describing the adsorption kinetic of MDIIP towards chromium species ions. Therefore, the adsorption process conforms to the pseudo-second-order kinetic model, which reveals that chemical adsorption is the control step during the adsorption process [54].

3.2.6. Adsorption mechanism

As mentioned earlier, the adsorption process of MDIIP to Cr(VI) and Cr(III) accords with the Langmuir isotherm and the pseudo-second-order kinetic model, which suggests that the adsorption occurs on the surface of adsorbent, and chemical adsorption is the dominant limiting step of adsorption. MDIIP has specific recognition ability for template ions due to the presence of cavities that match their shape and size. Essentially, for MDIIP, there are electrostatic attraction to inorganic chromium species (including Cr(VI) and Cr(III)) and coordination to Cr(III) at their respective optimal pH. The tertiary amino groups on the pyridine ring are protonated and carry positive charges, and generate electrostatic attractions with $HCrO_4^-$, CrO_4^{2-} and/or $Cr_2O_7^{2-}$ anions at pH 3.0. The carboxyl groups of MAA dissociate, carry negative charges, and generate electrostatic attractions with Cr^{3+} at pH 6.0. Meanwhile, the coordination interaction of the oxygen atom in –COOH and the nitrogen atom in tertiary amino group of pyridyl contributes to the adsorption of Cr^{3+}. To better analyze the adsorption mechanism of Cr(VI) and Cr(III) on MDIIP,

XPS was adopted to further analyze existing forms of chromium ions on MDIIP after adsorption by batch experiments. Fig. S7A shows that after the adsorption of Cr(VI), the new peaks at 575.2, 579.0 and 583.2 eV are attributed to CrO_4^{2-}, and 572.5 and 588.6 eV to $Cr_2O_7^{2-}$. The new peaks at 572.7, 576.1, 578.5, 582.5 and 588.5 eV are attributed to Cr $(COO)_n^{(3-n)+}$, $Cr(CO)^{3+}$, $Cr(H_2O)^{3+}$, Cr^{3+}–N and Cr^{3+} respectively in Fig. S7B. The above results revealed that Cr(VI) and Cr(III) have been successfully loaded onto MDIIP respectively. Interestingly, the appearance of $Cr(COO)_n^{(3-n)+}$, $Cr(CO)^{3+}$ and Cr^{3+}–N demonstrated that there were coordination interaction between oxygen atom in carboxyl group of MAA and Cr^{3+}, and between tertiary amino group of pyridine ring in 4-VP and Cr^{3+}. This results are in good agreement with the XPS characterization of MDIIP before removing Cr(VI) and Cr(III) templates, verifying the reversible adsorption-desorption of MDIIP to Cr(VI) and Cr (III) under different conditions. Therefore, the interaction of MDIIP and Cr(III) is both electrostatic attraction and coordination interaction, and the coordination interaction may be lasting as the pH increases.

3.3. Effect of elution conditions on desorption performance

To quantitatively desorb the captured chromium species, various elution conditions were evaluated including concentrations of HNO_3 and $NH_3{\cdot}H_2O$, elution time and elution volume. It is noticed from Fig. 4A that Cr(VI) was absorbed very weakly by MDIIP at pH higher than 6.0, and therefore dilute $NH_3{\cdot}H_2O$ solution was employed as the eluent for desorption of Cr(VI). In contrast, Cr(III) had poor adsorption at pH lower than 4.0, and therefore dilute HNO_3 solution was employed as the eluent for desorption of Cr(III).

Subsequently, 0.5 mL various concentrations of $NH_3{\cdot}H_2O$ (0.5, 0.75, 1.0, 1.5 mol L^{-1}) were used to elute Cr(VI) from the adsorbent. The recovery was increased to 95% as $NH_3{\cdot}H_2O$ concentration changed from 0.5 to 0.75 mol L^{-1}, and then reached a platform on further increasing the concentration as shown in Fig. S8A, and finally 1.0 mol L^{-1} $NH_3{\cdot}H_2O$ solution was chosen as the eluent for desorption of Cr(VI). Similarly, 0.5 mL various concentrations of HNO_3 (5, 7.5, 10, 15% (v/v)) were used to elute Cr(III) from the adsorbent. The recovery reached the highest at 7.5% and then remained unchanged as shown in Fig. S8B, and finally 10% (v/v) HNO_3 was chosen.

Fig. S8C indicated that the recoveries of Cr(VI) and Cr(III) were respectively increased with increasing elution time from 1 to 10 min, and then remained unchanged. Therefore, the elution time was set to 10 min for the two chromium species.

Meanwhile, Fig. S8D indicated that the recoveries of Cr(VI) and Cr (III) were respectively remained almost unchanged with increasing elution volume from 0.3 to 1.0 mL. Therefore, the eluent volume was set to 0.5 mL considering the enrichment factors.

3.4. Evaluation of freezing grinding process

The prepared bifunctionalized ion-imprinted nanocomposite, MDIIP, is a promising MSPE material to solve the problem in selectivity and stability of labile inorganic chromium species during separation and enrichment process. Before MSPE, however, the dissolution and extraction of these two species ions from complex solid samples in environment is still facing the issue of transformation each other, or change to other chromium species. In order to assess the influence of the liquid nitrogen freezing grinding process on the chromium species in real-world samples, quartz sand (120-180 mesh) was chosen as a simulated soil. The quartz sand powders were soaked in a mixed solution of Cr(VI) and Cr(III) at 50 mg L^{-1} each overnight, and then frozen-ground for 5, 10, 15, 20 and 25 cycles respectively. The adsorption amounts of Cr(VI) and Cr(III) was obtained by calculating the difference between the concentrations in supernatant and the original solution. Afterwards, Cr(VI) and Cr(III) in quartz sand powders (1.000 g) were extracted by water, MSPE separated with MDIIP, and detected by ICP-MS according to the proposed procedures described in 2.2 and 2.3. The dependence of the recoveries of two chromium species, based on the ratios of extracted to the adsorbed amounts, upon the number of freezing grinding cycles was shown in Fig. 5. The results indicated that 15 cycles are sufficient to fully grind and dry the quartz sands, and that the freezing grinding does not affect inorganic chromium species as time goes on until 25 cycles. Therefore, freeze grinding for 15 cycles was adopted as the pretreatment method for soil and leaf samples in subsequent experiment.

3.5. Performance of DIIP-MSPE-ICP-MS method

3.5.1. Anti-interference ability

In order to estimate the practical application potential of MDIIP, the coexisting anions, NO_3^-, PO_4^{3-} and SO_4^{2-}, cations, Na^+, Mg^{2+}, Ca^{2+}, Fe^{3+}, Ni^{2+}, Cu^{2+}, Zn^{2+} and Pb^{2+}, and humic acid widely present in the environment, were introduced to test the effects of these substances on the separation and enrichment of chromium species by DIIP-MSPE. Firstly, the background concentrations or contents of the above anions, cations and humic acid in actual water, soil and leaf samples were determined by ion chromatography, ICP-MS and UV-vis spectrophotometry, respectively. The results are summarized in Table S3. The specific steps for determining trace humic acid using UV-vis spectrophotometry referred to the literature [55]. Afterwards, 5 mL 30 μg L^{-1} of Cr(VI) or Cr(III) solution containing different concentrations or contents of the interfering substances was treated under the proposed conditions as mentioned in 2.2 and 2.3, and the results are shown in Table S4. The recoveries of Cr(VI) and Cr(III) were still in the range of 87.8-97.8% and 91.1-97.9% respectively in the presence of 60 mg L^{-1} Ca^{2+}, 50 mg L^{-1} Na^+, 30 mg L^{-1} NO_3^-, 15 mg L^{-1} SO_4^{2-}, 10 mg L^{-1} PO_4^{3-}, 5 mg L^{-1} Zn^{2+}, Mg^{2+} and humic acid, and 1 mg L^{-1} Ni^{2+}, Pb^{2+}, Cu^{2+} and Fe^{3+}. Thereby, this DIIP-MSPE-ICP-MS method demonstrates excellent anti-interference capability for chromium speciation analysis in real environmental samples.

3.5.2. Reusability

Under the optimized MSPE conditions, the MDIIP showed excellent reusability over five cycles with stable recovery of both Cr species (Fig. S9). The organic-inorganic hybrid monolithic interlayer offers good chemical resistant property and firm rigid configuration to the MDIIP. This is particularly important to the elemental speciation based on ion imprinting polymers.

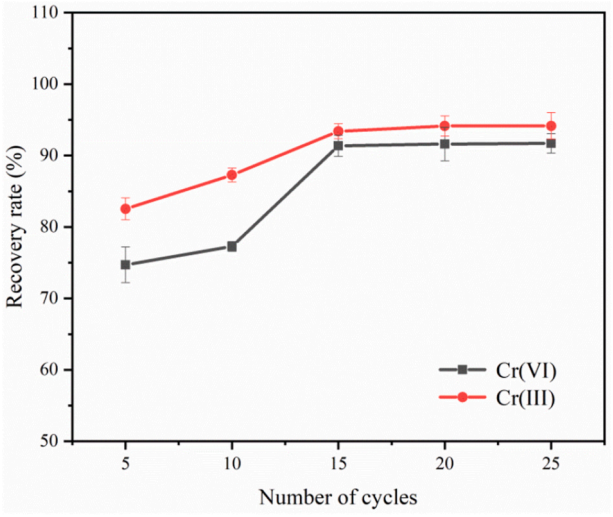

Fig. 5. The influence of the number of freezing grinding cycles on the extraction of inorganic chromium species.

3.5.3. Analytical merits

The DIIP-MSPE-ICP-MS protocol showed a linear range of 0.1-100 μg L^{-1} for Cr(VI) and Cr(III) ($R^2 = 0.9958$ and 0.9929, respectively), with LODs (S/N = 3) of 0.018 and 0.019 μg L^{-1}, respectively, at an enrichment factor of 10.

This method was validated using mixed standard solutions (S1–S3), environmental water certified reference material (CRM) (BY400024) and soil CRM (TMQC0181). In all cases, the determined concentrations or contents of Cr(VI), Cr(III) and total Cr were in excellent agreement with the reference values (Tables S5 and S6).

Finally, the applicability of the method was assessed by analyzing Cr (VI) and Cr(III) in actual samples, drinking (tap) and environmental (lake and river) waters samples, soil, leaves (Table 2). Moreover, two (for water) or three (for soil and leaf sample) different concentrations of standard Cr(VI) and Cr(III) solutions were spiked. As shown in Table S7, the recoveries for Cr(VI) and Cr(III) in all spiked samples ranged from 78.3% to 107.0% and from 76.0 to 98.8% respectively. In comparison with similar methods reported previously (Table S8), the proposed MDIIP-based analytical approach is established as a reliable and practical method for chromium speciation in complex environmental matrices.

4. Conclusions

A magnetic pyridyl- and carboxyl-bifunctionalized ion-imprinted polymer were prepared with 4-VP-$Cr_2O_7^{2-}$ and MAA-Cr^{3+} as double templates for the first time. The homogeneity in nano dimension came from the solvothermal-generated Fe_3O_4 nanoparticles as the cores. Then this MDIIP was used as an efficient MSPE matrix for speciation analysis of inorganic chromium with excellent recognition selectivity due to the specific imprinting sites on the surface of MDIIP. Moreover, Cr(VI) and Cr(III) can be captured by tertiary amino- and carboxyl-groups of the sole MDIIP adsorbent at different solution pH, respectively via electrostatic interaction, and synergetic electrostatic and coordination interactions. Afterwards, these two species were eluted under alkaline and acidic conditions respectively. Benefitting from the good chemical and mechanical stability of the MDIIP attributed to the organic-inorganic hybrid monolithic interlayer formed via sol-gel process, the adsorption efficiency towards Cr(VI) and Cr(III) kept unchanged after at least five times reuse, indicating the good reproducibility and economic profit. Very importantly, the stability of inorganic chromium species was preserved during the whole separation-enrichment process because a freezing grinding operation was utilized to dissolute and extract Cr(VI) and Cr(III) from samples analyzed but no oxidation and reduction operation was pre-executed, and mild loading and elution conditions were employed in the subsequent DIIP-MSPE process. To the best of our knowledge, this work represents the first report on a magnetic bifunctionalized ion-imprinted polymer (MDIIP) for the speciation analysis of inorganic chromium. Validated by CRMs and spike-recovery tests, the developed MSPE-ICP-MS method was successfully applied to determine chromium species in diverse real samples, including drinking and environmental waters, soil and leaves. Given the above experimental results, this MDIIP-based elemental speciation approach has higher application potential in the separation and enrichment of different metallic and submetallic species.

CRediT authorship contribution statement

Yi-Fan Pan: Writing – original draft, Visualization, Methodology, Investigation, Formal analysis. **Sen Zhang:** Visualization, Methodology, Data curation. **Jing Yang:** Visualization, Data curation. **Xiao-Bing Cui:** Visualization, Resources, Formal analysis. **Hong-Zhen Lian:** Writing – review & editing, Supervision, Project administration, Funding acquisition, Conceptualization.

Table 2
Analytical results of Cr(VI) and Cr(III) in drinking and environmental waters, and soil and leaf samples.

Sample	Found		RSD (%)	
	Cr(VI)	Cr(III)	Cr(VI)	Cr(III)
Tap water (μg L^{-1})	0.09 ± 0.01	0.02 ± 0.01	4.4	3.1
Lake water (μg L^{-1})	0.15 ± 0.02	0.01 ± 0.01	3.3	2.7
River water (μg L^{-1})	0.01 ± 0.01	0.01 ± 0.01	1.6	4.0
Soil (mg kg^{-1})	3.86 ± 0.34	38.7 ± 0.10	5.0	2.7
Leaf (mg kg^{-1})	22.9 ± 1.98	7.37 ± 0.69	8.6	9.4

Declaration of competing interest

The authors declare that they have no known competing financial interests or personal relationships that could have appeared to influence the work reported in this paper.

Acknowledgements

This work was supported by the National Natural Science Foundation of China (22176085 and 21874065).

Appendix A. Supplementary data

Supplementary data to this article can be found online at https://doi.org/10.1016/j.aca.2026.345407.

Data availability

Data will be made available on request.

References

[1] A.D. Dayan, A.J. Paine, Mechanisms of chromium toxicity, carcinogenicity and allergenicity: review of the literature from 1985 to 2000, Hum. Exp. Toxicol. 20 (9) (2001) 439–451, https://doi.org/10.1191/096032701682693062.
[2] H. Karimi-Maleh, A. Ayati, S. Ghanbari, Y. Orooji, B. Tanhaei, F. Karimi, M. Alizadeh, J. Rouhi, L. Fu, M. Sillanpää, Recent advances in removal techniques of Cr(VI) toxic ion from aqueous solution: a comprehensive review, J. Mol. Liq. 329 (2021) 115062, https://doi.org/10.1016/j.molliq.2020.115062.
[3] S. Prasad, K.K. Yadav, S. Kumar, N. Gupta, M.M.S. Cabral-Pinto, S. Rezania, N. Radwan, J. Alam, Chromium contamination and effect on environmental health and its remediation: a sustainable approaches, J. Environ. Manag. 285 (2021) 112174, https://doi.org/10.1016/j.jenvman.2021.112174.
[4] M. Owlad, M.K. Aroua, W.A.W. Daud, S. Baroutian, Removal of hexavalent chromium-contaminated water and wastewater: a review, Water Air Soil Pollut. 200 (2009) 59–77, https://doi.org/10.1007/s11270-008-9893-7.
[5] R.T. Kapoor, M.F. Bani Mfarrej, P. Alam, J. Rinklebe, P. Ahmad, Accumulation of chromium in plants and its repercussion in animals and humans, Environ. Pollut. 301 (2022) 119044, https://doi.org/10.1016/j.envpol.2022.119044.
[6] N. Shevchenko, V. Zaitsev, A. Walcarius, Bifunctionalized mesoporous silicas for Cr (VI) reduction and concomitant Cr(III) immobilization, Environ. Sci. Technol. 42 (2008) 6922–6928, https://doi.org/10.1021/es800677b.
[7] G. Quievryn, J. Messer, A. Zhitkovich, Carcinogenic chromium(VI) induces cross-linking of vitamin C to DNA in vitro and inhuman lung A549 cells, Biochemistry 41 (2002) 3156–3167, https://doi.org/10.1021/bi011942z.
[8] J. He, X. Qian, R. Carpenter, Q. Xu, L. Wang, Y. Qi, Z.X. Wang, L.Z. Liu, B.H. Jiang, Repression of miR-143 mediates Cr(VI)-induced tumor angiogenesis via IGF-IR/IRSI/ERK/IL-8pathway, Toxicol. Sci. 134 (2013) 26–38, https://doi.org/10.1093/toxsci/kft101.
[9] J. Dai, Y. Ji, W. Wang, D. Kim, L.Y. Fai, L. Wang, J. Luo, Z. Zhang, Loss of fructose-1, 6-bisphosphatase induces glycolysis and promotes apoptosis resistance of cancer stem-like cells: an important role in hexavalent chromium-induced carcinogenesis, Toxicol. Appl. Pharmacol. 331 (2017) 164–173, https://doi.org/10.1016/j.taap.2017.06.014.
[10] F. Yang, L. Zhao, D. Mei, L. Jiang, C. Geng, Q. Li, X. Yao, Y. Liu, Y. Kong, J. Cao, HMGA2 plays an important role in Cr(VI)-induced autophagy, Mol. Cancer 141 (2017) 986–997, https://doi.org/10.1002/ijc.30789.
[11] S. Ali, S.A. Bharwana, M. Rizwan, M. Farid, S. Kanwal, Q. Ali, M. Ibrahim, R.A. Gill, M.D. Khan, Fulvic acid mediates chromium (Cr) tolerance in wheat (Triticum aestivum L.) through lowering of Cr uptake and improved antioxidant defense system, Environ. Sci. Pollut. Res. Int. 22 (2015) 10601–10609. https://link.springer.com/article/10.1007/s11356-015-4271-7.
[12] World Health Organization, Chromium in Drinking-water: background document for development of WHO guidelines for drinking-water quality. https://iris.who.int

/bitstream/handle/10665/338062/WHO-HEP-ECH-WSH-2023.3-eng.pdf/, 2023. (Accessed 3 March 2023).
[13] National standard of the People's Republic of China, standards for drinking water quality, GB5749-2022, https://openstd.samr.gov.cn/bzgk/gb/newGblnfo?hcno=99E9C17E3547A5743C0CE2FD1FFD9F2F7BE/, 2022. (Accessed 15 March 2022).
[14] Environmental Protection Agency, Chromium in Drinking Water, 2022. https://www.epa.gov/sdwa/chromium-drinking-water/. (Accessed 3 March 2022).
[15] National standard of the People's Republic of China, soil environmental quality-Risk control standard for soil contamination of development land, GB36600-2018, https://www.mee.gov.cn/ywgz/fgbz/bz/bzwb/trhj/202307/W020190626596188930731.pdf, 2023. (Accessed 22 June 2023).
[16] E. Birlik, A. Ersöz, E. Açikkalp, A. Denizli, R. Say, Cr(III)-imprinted polymeric beads: sorption and preconcentration studies, J. Hazard. Mater. 140 (2007) 110–116, https://doi.org/10.1016/j.jhazmat.2006.06.141.
[17] B. Dhal, H.N. Thatoi, N.N. Das, B.D. Pandey, Chemical and microbial remediation of hexavalent chromium from contaminated soil and mining/metallurgical solid waste: a review, J. Hazard. Mater. 250 (2013) 272–291, https://doi.org/10.1016/j.jhazmat.2013.01.048.
[18] C.F. Ding, X.G. Li, T.L. Zhang, Y.B. Ma, X.X. Wang, Phytotoxicity and accumulation of chromium in carrot plants and the derivation of soil thresholds for Chinese soils, Ecotoxicol. Environ. Saf. 108 (2014) 179–186, https://doi.org/10.1016/j.ecoenv.2014.07.006.
[19] H.P. Li, Y.Q. Zhang, S.W. Li, Y.S. Wang, H.L. Li, Toxicity of chromium to wheat (Triticum aestivum L.) in two soils: influence of soil properties and chromium form, Environ. Sci. Pollut. Res. 30 (2023) 100466–100476, https://doi.org/10.1007/s11356-023-29383-y.
[20] M.B. Hansen, T. Menné, J.D. Johansen, Cr(III) reactivity and foot dermatitis in Cr (VI) positive patients, contact, Dermatitis 54 (3) (2006) 140–144, https://doi.org/10.1111/j.0105-1873.2006.00802.x.
[21] J.W. Wang, Z.J. Fang, J. Gao, L.J. Sun, Y.L. Wang, Y. Liu, R. Gooneratne, Comparative study of cytotoxicity, DNA damage and oxidative stress induced by heavy metals Cd(II), Hg(II) and Cr(III) in yeast, Curr. Microbiol. 78 (2021) 1856–1863, https://doi.org/10.1007/s00284-021-02454-4.
[22] O.D. Uluozlu, M. Tuzen, D. Mendil, B. Kahveci, M. Soylak, 3-Ethyl-4-(p-chlorobenzylidenamino-4,5-dihydro-1H-1,2, 4-triazol-5-one (EPHBAT) as precipitant for carrier element free coprecipitation and speciation of chromium(III) and chromium(VI), J. Hazard. Mater. 172 (2009) 395–399, https://doi.org/10.1016/j.jhazmat.2009.07.021.
[23] R. Pechancová, R.J.N.B. Silva, D. Milde, T. Pluháček, Bottom-up measurement uncertainty evaluation for Cr(III) and Cr(VI) speciation in natural water by HPLC-ICP-MS, Microchem. J. 212 (2025) 113190, https://doi.org/10.1016/j.microc.2025.113190.
[24] G.D. Matos, E.B. dos Reis, A.C.S. Costa, S.L.C. Ferreira, Speciation of chromium in river water samples contaminated with leather effluents by flame atomic absorption spectrometry after separation/preconcentration by cloud point extraction, Microchem. J. 92 (2009) 135–139, https://doi.org/10.1016/j.microc.2009.02.009.
[25] Y.F. Huang, Y. Li, Y. Jiang, X.P. Yan, Magnetic immobilization of amine-functionalized magnetite microspheres in a knotted reactor for on-line solid-phase extraction coupled with ICP-MS for speciation analysis of trace chromium, J. Anal. At. Spectrom. 25 (2010) 1467–1474.
[26] H. Shirkhanloo, A.F. Zarandi, M. Faraji, Food analysis: n-benzyl-n-methyl thiourea immobilized on multi-walled carbon nanotubes for speciation of chromium in food and water samples using ultrasound-assisted heterogeneous suspension IL-micro-solid-phase extraction, Food Chem. 508 (2026) 148369, https://doi.org/10.1016/j.foodchem.2026.148369.
[27] H.M. Jiang, T. Yang, Y.H. Wang, H.Z. Lian, X. Hu, Magnetic solid-phase extraction combined with graphite furnace atomic absorption spectrometry for speciation of Cr(III) and Cr(VI) in environmental waters, Talanta 116 (2013) 361–367, https://doi.org/10.1016/j.talanta.2013.05.008.
[28] P. Li, Y.J. Chen, H.Z. Lian, X. Hu, A centrifugal microfluidic platform integrating monolithic capillary columns for high-throughput speciation of chromium, J. Anal. At. Spectrom. 29 (2014) 1785–1790, https://doi.org/10.1039/C4JA00149D.
[29] H.Y. Peng, N. Zhang, M. He, B.B. Chen, B. Hu, Simultaneous speciation analysis of inorganic arsenic, chromium and selenium in environmental waters by 3-(2-aminoethylamino) propyltrimethoxysilane modified multi-wall carbon nanotubes packed microcolumn solid phase extraction and ICP-MS, Talanta 131 (2015) 266–272, https://doi.org/10.1016/j.talanta.2014.07.054.
[30] L.Y. Zhao, J.J. Fei, H.Z. Lian, L. Mao, X.B. Cui, Simultaneous speciation analysis of chromium and antimony by novel carboxyl-functionalized hybrid monolithic column solid phase microextraction coupled with ICP-MS, J. Anal. At. Spectrom. 34 (2019) 1693–1700, https://doi.org/10.1039/C9JA00157C.
[31] Q.Y. Zhu, L.Y. Zhao, D. Sheng, Y.J. Chen, X. Hu, H.Z. Lian, L. Mao, X.B. Cui, Speciation analysis of chromium by carboxylic group functionalized mesoporous silica with inductively coupled plasma mass spectrometry, Talanta 195 (2019) 173–180, https://doi.org/10.1016/j.talanta.2018.11.043.
[32] Y.L. Sun, L.Y. Zhao, H.Z. Lian, L. Mao, X.B. Cui, Carboxyl-functionalized hybrid monolithic column prepared by "Thiol-ene" click reaction for noninvasive speciation analysis of chromium with inductively coupled plasma-mass spectrometry, Anal. Chim. Acta 1137 (2020) 85–93, https://doi.org/10.1016/j.aca.2020.08.052.
[33] F. Faiz, Y.F. Pan, S. Zhang, J.X. Dai, J.Q. Qiao, H.Z. Lian, L. Mao, X.B. Cui, A novel zwitterionic magnetic nanocomposite developed for non-invasive speciation analysis of inorganic chromium, J. Hazard. Mater. 474 (2024) 134860, https://doi.org/10.1016/j.jhazmat.2024.134860.
[34] H.E.H. Ahmed, M. Soylak, A MWCNTs@$CuAl_2O_4$@SiO_2 nanocomposite for the speciation of Cr(III), Cr(VI), and total chromium prior to high-resolution continuum source flame atomic absorption spectrometric determination, Water Air Soil Pollut. 235 (2024) 217, https://doi.org/10.1007/s11270-024-07020-9.
[35] Z. Erbas, O. Ozalp, A.A. Matin, M. Soylak, Speciation of chromium by magnetic solid phase microextraction using an activated charcoal-molybdenum (IV) selenide-magnetite composite with flame atomic absorption spectrometric (FAAS) detection, Anal. Lett. 57 (2024) 2727–2744, https://doi.org/10.1080/00032719.2023.2301502.
[36] F.L. Silva, G.L. Scheel, M.G. Segatelli, C.R.T. Tarley, Preconcentration/speciation of chromium by using nanocomposites based on carbon nanotubes and functional polymers, Composite Nanoadsorbent. (2019) 139–180, https://doi.org/10.1016/B978-0-12-814132-8.00008-3.
[37] L.Y. Zhao, J.J. Fei, H.Z. Lian, L. Mao, X.B. Cui, Development of a novel amine- and carboxyl-bifunctionalized hybrid monolithic column for non-invasive speciation analysis of chromium, Talanta 212 (2020) 120799, https://doi.org/10.1016/j.talanta.2020.120799.
[38] K. Mosbach, Molecular imprinting, Trends Biochem. Sci. 19 (1994) 9–14, https://doi.org/10.1016/0968-0004(94)90166-x.
[39] M. Berghaus, R. Mohammadi, B. Sellergren, Productive encounter: molecularly imprinted nanoparticles prepared using magnetic templates, Chem. Commun. 50 (2014) 8993–8996, https://doi.org/10.1039/C4CC01346H.
[40] J. Kupai, E. Rojik, P. Huszthy, G. Szekely, Role of chirality and macroring in imprinted polymers with enantiodiscriminative power, ACS Appl. Mater. Interfaces 7 (2015) 9516–9525, https://doi.org/10.1021/acsami.5b00755.
[41] M. Yoshikawa, K. Tharpa, S.O. Dima, Molecular imprinted membranes: past, present, and future, Chem. Rev. 116 (2016) 11500–11528, https://doi.org/10.1021/acs.chemrev.6b00098.
[42] A. Cecchini, V. Raffa, F. Canfarotta, G. Signore, S. Piletsky, M.P. Macdonald, A. Cuschieri, In vivo recognition of human vascular endothelial growth factor by molecularly imprinted polymers, Nano Lett. 17 (2017) 2307–2312, https://doi.org/10.1021/acs.nanolett.6b05052.
[43] J.Q. Fu, L.X. Chen, J.H. Li, Z. Zhang, Current status and challenges of ion imprinting, J. Mater. Chem. A 3 (2015) 13598–13627, https://doi.org/10.1039/C5TA02421H.
[44] I. Karadjova, I. Dakova, T. Yordanova, P. Vasileva, Nanomaterials for elemental speciation, J. Anal. At. Spectrom. 31 (2016) 1949–1973, https://doi.org/10.1039/C6JA00168H.
[45] M. He, L. Huang, B. Zhao, B. Chen, B. Hu, Advanced functional materials in solid phase extraction for ICP-MS determination of trace elements and their species – a review, Anal. Chim. Acta 973 (2017) 1–24, https://doi.org/10.1016/j.aca.2017.03.047.
[46] Y. Liu, X. Meng, J. Han, Z. Liu, M. Meng, Y. Wang, R. Chen, S. Tian, Speciation, adsorption and determination of chromium(III) and chromium(VI) on a mesoporous surface imprinted polymer adsorbent by combining inductively coupled plasma atomic emission spectrometry and UV spectrophotometry, J. Separ. Sci. 36 (2013) 3949–3957, https://doi.org/10.1002/jssc.201300972.
[47] R. Huang, X. Ma, X. Li, L. Guo, X. Xie, M. Zhang, J. Li, A novel ion-imprinted polymer based on graphene oxide-mesoporous silica nanosheet for fast and efficient removal of chromium (VI) from aqueous solution, J. Colloid Interface Sci. 514 (2018) 544–553, https://doi.org/10.1016/j.jcis.2017.12.065.
[48] Z. Kong, Y. Du, J. Wei, H. Zhang, L. Fan, Synthesis of a new ion-imprinted polymer for selective Cr(VI) adsorption from aqueous solutions effectively and rapidly, J. Colloid Interface Sci. 588 (2021) 749–760, https://doi.org/10.1016/j.jcis.2020.11.107.
[49] X. Qi, S. Gao, G.S. Ding, A.N. Tang, Synthesis of surface Cr (VI)-imprinted magnetic nanoparticles for selective dispersive solid-phase extraction and determination of Cr (VI) in water samples, Talanta 162 (2017) 345–353, https://doi.org/10.1016/j.talanta.2016.10.040.
[50] S. Zhang, S. Wang, X. Shan, Effect of sample pretreatment upon the metal speciation in sediments by a sequential extraction procedure, Chem. Speciat. Bioavailab. 13 (2001) 69–74, https://doi.org/10.3184/095422901782775435.
[51] F. Faiz, J.Q. Qiao, H.Z. Lian, L. Mao, X.B. Cui, A combination approach using two functionalized magnetic nanoparticles for speciation analysis of inorganic arsenic, Talanta 237 (2022) 122939, https://doi.org/10.1016/j.talanta.2021.122939.
[52] N.K. Hamadi, X.D. Chen, M.M. Farid, M.G.Q. Lu, Adsorption kinetics for the removal of chromium (VI) from aqueous solution by adsorbents derived from used tyres and sawdust, Chem. Eng. J. 84 (2001) 95–105, https://doi.org/10.1016/S1385-8947(01)00194-2.
[53] Z. Zhou, X. Liu, M. Zhang, J. Jiao, H. Zhang, J. Du, B. Zhang, Z. Ren, Preparation of highly ion-imprinted polymers with Fe_3O_4 nanoparticles as carrier for removal of Cr(VI) from aqueous solution, Sci. Total Environ. 699 (2020) 134334, https://doi.org/10.1016/j.scitotenv.2019.134334.
[54] Z.Q. Ren, J. Wang, H.W. Zhang, F. Zhang, S.C. Tian, Z.Y. Zhou, Adsorption of rubidium ion from aqueous solution by surface ion imprinted materials, Chin. J. Chem. Eng. 54 (2023) 1–10, https://doi.org/10.1016/j.cjche.2022.04.011.
[55] B. Yuan, S. Lü, W.H. Zhang, Determination of trace humic acid in water by UV spectrophotometry, Ind. water Treat. 30 (2010) 75–77. https://www.cnki,net.